Journal of Applied Mechanics and Technical Physics, Vol. 42, No. 2, pp. 300–309, 2001

"INVISCID FINGER" INSTABILITY IN REGULAR MODELS OF A POROUS MEDIUM

A. P. Ershov, A. Ya. Dammer, and A. L. Kupershtokh

UDC 532.546.2:532.685

Displacement of a fluid from a porous medium is considered. The flow is assumed to be fast enough, i.e., the Reynolds number based on the characteristic pore size is large. If the driving fluid is less dense (for example, a gas), the interface is unstable. This instability is similar to the well-known viscous finger instability but the governing parameter is density instead of viscosity. The instability is demonstrated experimentally using two-dimensional models. In square lattices of perpendicular channels, noticeable branching of fingers is not observed, which is attributed to the anisotropy of such an artificial porous medium. A more ordinary pattern with finger branching is obtained in a two-dimensional layer of spheres, which appears to be more isotropic. A simple model describing flow in a square lattice is proposed. The initial stage of growth is considered, and the instability increment is estimated. A qualitative analysis of the nonlinear stage is performed.

Introduction. We first consider the classical problem of displacement of a viscous fluid. In a porous medium there is an interface between the viscous fluid and the relatively inviscid fluid. The simplest is the extreme case where the viscosity of the displacing fluid is negligible. In the viscous region with a low flow rate $\boldsymbol{u}$, a linear filtration law is valid:

$$\boldsymbol{u} = -K\nabla p/\mu. \tag{1}$$

Here p is the pressure, K is the permeability of the medium, and μ is the fluid viscosity. The continuity condition $\nabla \cdot \boldsymbol{u} = 0$ leads to the Laplace equation

$$\Delta p = 0. \tag{2}$$

Within the inviscid region, the pressure is uniform. Hence, on the moving interface, the pressure is also constant. Using this boundary condition, one finds a solution of the Laplace equation in the viscous region. Then, the velocity of the interface is determined from (1), and the displacement process can be calculated.

If a viscous fluid is displaced by a relatively inviscid fluid, the interface is subjected to Saffman–Taylor instability [1]. When a bulge appears at the interface, the pressure gradient near it increases, and the flow velocity and, hence, the interface velocity also increase. As a result, the bulge grows. The "fingers" of the inviscid fluid burst ahead.

In many experiments, following those described in [1], viscous fingers were studied using a Hele Shaw cell, in which a fluid flows in a narrow gap between two parallel planes. In Hele Shaw cells, wide smooth fingers form because short-wave instability is suppressed by surface tension. In a rectangular cell, the leading finger inhibits the growth of neighbors. As a result, the finger that "survived" occupies approximately half of the cell. Paterson [2] showed that in a radial Hele Shaw cell, fingers branch off when a critical width is reached. This width is also determined by surface tension, and the shape of the fingers is still smooth.

Lavrent'ev Institute of Hydrodynamics, Siberian Division, Russian Academy of Sciences, Novosibirsk 630090. Translated from Prikladnaya Mekhanika i Tekhnicheskaya Fizika, Vol. 42, No. 2, pp. 129–140, March–April, 2001. Original article submitted October 14, 1999; revision submitted April 4, 2000.

 0021-8944/01/4202-0300 $25.00

Måløy et al. [3] used a more realistic model — a layer of an artificial porous medium between two transparent disks. In this cell, a different pattern of radial displacement was obtained. The finger width is determined by the pore size. As the fingers grow, their tips produce branches, and thin ramified structures thus develop. Lenormand et al. [4] studied displacement in a rectangular cell and obtained similar shapes. When surface tension can be ignored, similar patterns are also observed in Hele Shaw cells [5]. These results confirmed the analogy between viscous displacement and diffusion-limited aggregation (DLA), noted by Paterson [6]. The DLA process, introduced by Witten and Sander [7, 8], involves the formation of a cluster of small particles diffusing to the cluster boundary surface. Steady-state diffusion, as well as linear filtration, is described by the Laplace equation, and the boundary of the cluster grows at a rate proportional to the concentration gradient. In the DLA process, branched structures form that are reproduced in stochastic growth models. Similar problems are encountered in studies of electrical breakdown with pressure replaced by potential. An equipotential system of discharge channels acts as the inviscid fluid. Application of the DLA-type models to breakdown is described in [9].

Linear problems of the type of (1), (2) have been studied comprehensively. Instability of the interface leads to development of complex (fractal) structures. In particular, a cluster formed by jets of an inviscid fluid is described by the basic relation $M \sim R^D$. Here M is the mass of the cluster (or its volume) and R is its characteristic size. The exponent D is the fractal (fractional) dimension, which is smaller than the dimension of the embedding space. As a result, large clusters are highly rarefied. For example, for two-dimensional radial displacement, Måløy et al. [3] obtained a dimension of 1.62.

Nonlinear problems have received comparatively less attention. Niemeyer et al. [9] and Evertsz [10] simulated electrical breakdown assuming that the rate of growth of the discharge boundary is proportional to the electric field to power η. For $\eta \neq 1$, the boundary condition for growth was nonlinear but the spatial formulation of the problem remained linear (the Laplace equation was solved). Daccord et al. [5] explored the displacement of a non-Newtonian fluid assuming $u \sim \left|\nabla p\right|^m$, where $m > 1$.

For fast filtration, when the large Reynolds number calculated from the characteristic pore size is large, instead of the linear relation (1), the square resistance law (Forchgeimer regime) holds [11, 12]:

$$\rho \boldsymbol{u}|\boldsymbol{u}| = -f\nabla p. \tag{3}$$

Here ρ is the fluid density and f is a constant proportional to the pore size. For an incompressible fluid, the continuity condition leads to the following equation for pressure:

$$\nabla \cdot \left(\nabla p\left|\nabla p\right|^{-1/2}\right) = 0. \tag{4}$$

If the fluid is displaced by a low-density gas, the pressure gradient in the gas region is small, and the pressure on the interface is practically constant. The normal velocity of the interface is proportional to $\left|\nabla p\right|^{1/2}$.

Qualitatively, the nonlinear problem (3), (4) is similar to the viscous displacement problem, and one might expect instability of the displacement (growth and branching of fingers). We can speak of "dense" or "inviscid" finger instability.

Problem (3), (4) was considered in [13]. The initial growth of initial small-amplitude perturbations was studied analytically, and the late stage of long fingers was analyzed numerically. The perturbations developed more slowly than in the "viscous" problem. This resulted in the formation of denser clusters than those in the Laplace case. Nevertheless, the region of displacement was fractal, although the fractal dimension was slightly larger in this case.

Inviscid instability in a porous medium is of particular interest. Situations where the flow is so fast that the simple approach (3), (4) is applicable are rather common. For example, this formulation describes approximately the filtration of combustion products in a porous energetic material. The high temperature of the products corresponds to their low density, and the gas (air) in the pore space acts as the displaced fluid. Instability of the interface can lead to the formation of flame jets that are extended forward.

It is of interest to determine whether in a real fast flow, structures of increasing complexity form, as is the case for viscous fractals [3], or a different type of instability dominates in which the flow geometry is

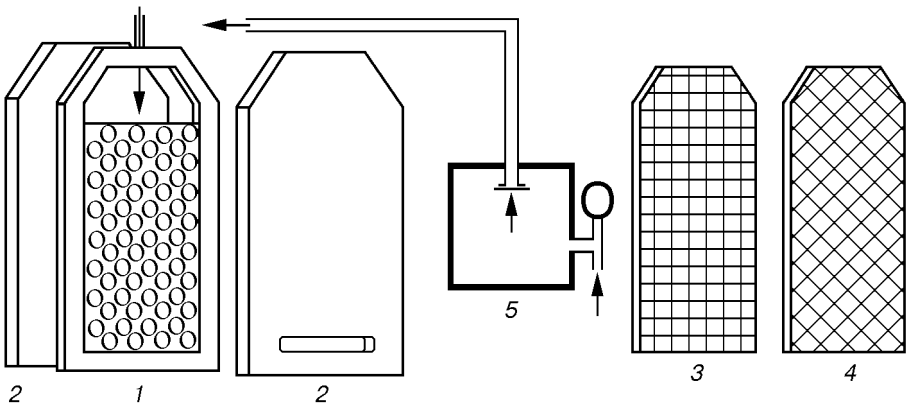

Fig. 1

progressively simplified [1]. The present paper reports experimental results obtained for nonlinear displacement and theoretical estimates. Focus is on displacement in regular anisotropic models of a porous medium. Anisotropy is practically inevitable for a two-dimensional model that represents a set of channels and obstacles: the process is easier to visualize in a two-dimensional layer.

It should be noted that flows in channel type models can differ markedly from flows in real porous media. Therefore, extension of results to the case of a natural (isotropic or anisotropic) medium is not always possible. Nevertheless, the use of model media is a natural first step in studies of filtration flows. In addition, model flows are of independent interest (similarly to Hele Shaw flows). Channel anisotropy can strongly affect combustion processes. Flame propagation in channel lattices was considered in, e.g., [14].

1. Experiment. Displacement of a dense liquid by a gas was visualized using a special cell (Fig. 1). A metal frame 1 and two thick Plexiglas walls 2 formed a chamber, in which a plane model of a porous medium was placed. One type of model (shown schematically in the frame) was a regular monolayer of identical steel spheres. Spheres of 2.5 or 12.2 mm diameter were used. The other type of model was a Plexiglas plate on one of whose sides a square lattice of channels simulating a pore space was grooved. The lattice period was $d = 6$ mm, and the depth and width of the channels were $\delta = 2$ mm. Figure 1 shows two inserts (3 and 4) with variously oriented channels. For longitudinal orientation, one of the lattice directions coincides with the direction of displacement. For diagonal orientation, the channels are cut at angles of $\pm 45^\circ$ to the direction of the main flow.

The cell was filled with a liquid. Air was pumped in container 5, which was connected to the cell through a valve (ruptured membrane). After opening of the valve, compressed air entered the cell and pushed the liquid. At the bottom of the chamber, openings connected the cell with a vessel which was filled with a liquid and plugged with a stopper. When the gas pressure was applied, the stopper went off, and the liquid was free to flow outside. The cross section of the openings was sufficient to neglect their hydraulic resistance. The driving air pressure (50–100 kPa) was more than an order of magnitude higher than the pressure of the liquid column in the cell. Deformation of the chamber by internal pressure was prevented by rigid fastening of rather thick (30 mm) walls. The assembly was carefully sealed to prevent leakage.

The capillary pressure jump at the interface was less than a percent of the driving pressure. In most experiments, the effect of gravity was negligible because the gravitational pressure drops did not exceed several percent of the driving pressure. However, the capillary and gravitational effects could be significant in some special cases described below.

The flow velocity was about 1 m/sec. The Reynolds number based on the channel diameter or the characteristic pore size was about several thousand. This means that the resistance law is nearly quadratic [15].

The cell had a width of $l = 20$ cm and a length of $L = 50$ cm. The compressed air volume (1 liter) maintained nearly constant pressure on the interface (for example, for a layer of small spheres, the pressure drop for displacement of half of the liquid column was lower than 10%). This condition was violated for a layer of 12.2-mm-diameter spheres because the cell volume was much larger.

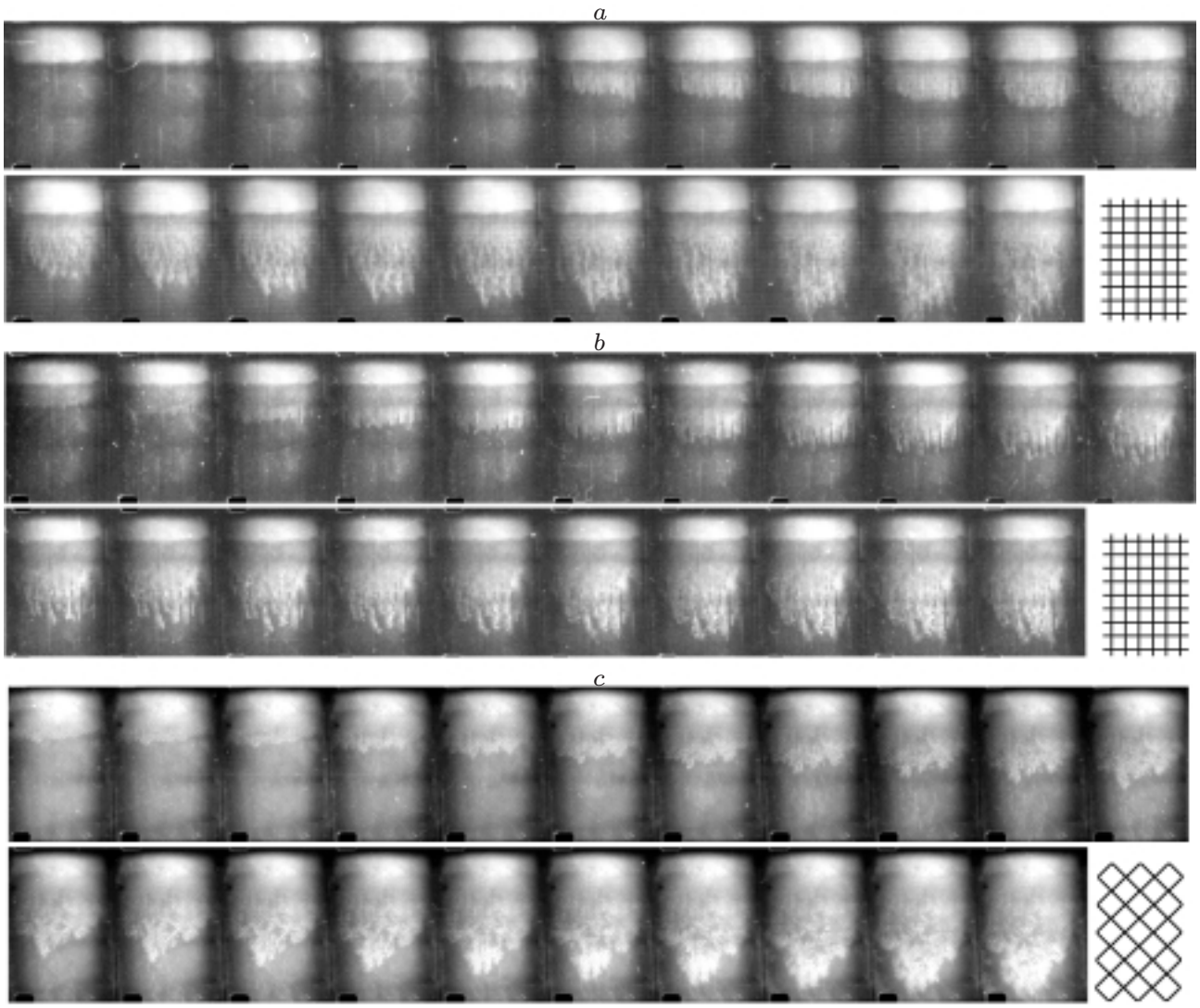

Fig. 2

The shape of the interface was observed by reflected or transmitted light using photography, frame camera or video recording. The working medium was tinted alcohol (in experiments with steel spheres) or tinted water.

Figure 2a shows the results of an experiment with a square lattice of channels. In each row, the frames are arranged from left to right, and the bottom row is a continuation of the top one. The shooting speed was 150 frames/sec. The excess air pressure was 70 kPa. The lattice orientation is longitudinal (shown schematically in Fig. 2).

The light region is air, and the pores filled with water are dark. Initially, the displacement was rather uniform. In about 1/15 sec (10 frames), one can clearly see perturbations at the displacement front, which then develop into narrow longitudinal jets. The number and shape of the jets vary from experiment to experiment.

Inspection of the frames shows that for longitudinal orientation, the liquid not only remains in the gaps between the jets but is locked in the transverse channels (the flow has a pronounced structure in the form of vertical strips). Surface tension is important here. For the horizontal direction, the relative role of capillary forces is specified by the ratio of the pressure gradients $(4\sigma/\delta)/(d|\partial p/\partial x|)$, where σ is the surface-tension

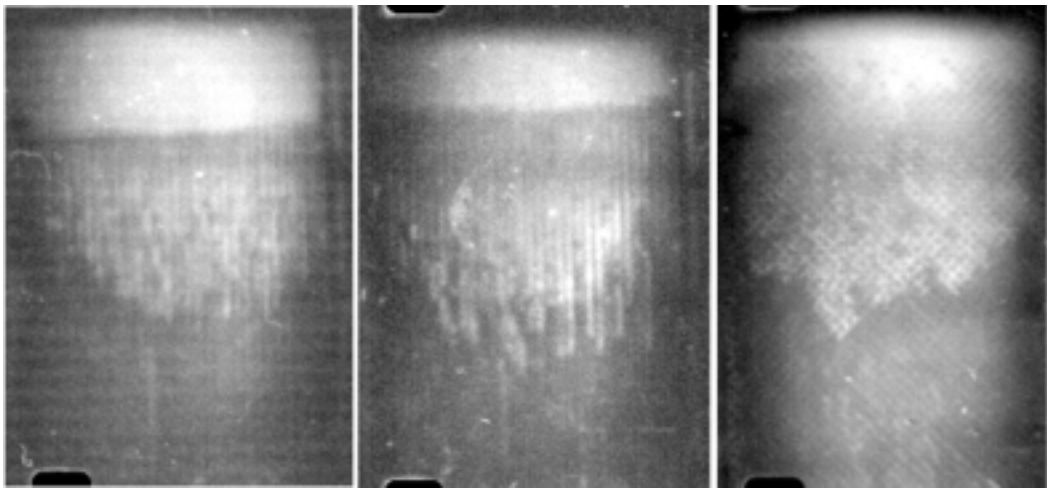

Fig. 3

coefficient. For the vertical gradient $\partial p/\partial y$ under experimental conditions, this quantity would be about 0.1. Because the horizontal gradient is far lower, surface menisci are able to hold the liquid in transverse channels between neighboring vertical channels that are already filled with air.

The liquid remaining in transverse channels can affect the result of the next experiment. Figure 2b shows records of an experiment in which above the level of complete filling there was a region of partly wetted pores (the gray band between the light dry air region and the dark gray liquid region in the first frame). This band remains practically unchanged and is visible in all frames, i.e., the liquid in transverse pores does not move. In this case, narrow fingers develop much faster (cf. Fig. 2a). Apparently, the residual liquid produces additional perturbations, for example, in the form of local obstacles to air flow.

Figure 2c shows a typical result of a "shot" with a diagonally oriented lattice. Here straightforward break of air in the direction of displacement is hindered because each channel ends with a wall. The pressure drop is the same as in Fig. 2a and b. The diagonal displacement is slower, but distortions of the front arise much faster. They also develop into protrusions. Instead of long thin jets, one can see wedges with about right front angles. These wedges become more pronounced as the perturbation amplitude increases.

Unlike in the longitudinal case, for the diagonal orientation, the displacement is practically complete although the liquid can remain in separate "pockets" behind the main front. Enlarged images of the rightmost frames in the top rows of Fig. 2a–c are given (from left to right) in Fig. 3. They clearly show the details mentioned above. In the first two snapshots, light horizontal bands are not observed, and the displacement fingers are narrow and long. The right frame clearly shows the lattice structure and wedges.

Hence, in a square lattice, a developed flow reflects its symmetry, and for both orientations, motion along the channels is preferred. If the channels are vertical, such flows start to develop immediately, and for the diagonal arrangement of channels, the fingers are rapidly transformed into wedges, whose boundaries move almost longitudinally.

The above results differ greatly from those obtained for slow viscous displacement where branching structures are formed [3–5]. The reason for the difference lies in the anisotropy of the medium and not in the resistance nonlinearity (which affects only the degree of branching [13]). Therefore, a series of experiment was performed with another model of a porous medium — a layer of spheres. This model appears more isotropic (in any way, its anisotropy is obviously different).

Figure 4 shows a static frame (at the left) and one of the flow stages (at the right) in a layer of 2.5-mm spheres. Air (dark region) propagates from top to bottom. The driving air pressure is 70 kPa. The cell plane is vertical. The flow direction is shown by an arrow. The light bands at the top of the frame are obstacles that equalize the air pressure action on the liquid.

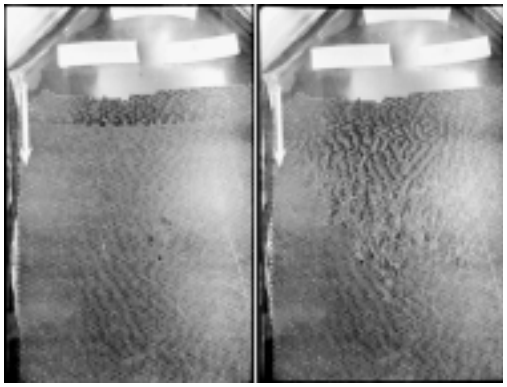

Fig. 4

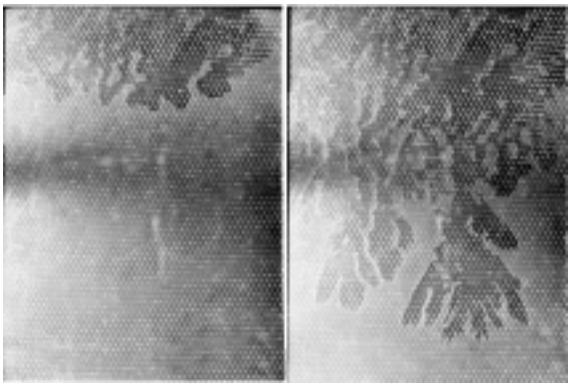

Fig. 5

Between the regular layer of spheres and the flat wall there are always three systems of "channels" that form equilateral triangles. The rows of spheres were laid from bottom upward so that in the horizontal direction, there were gaps and, what is more important for the flow, there were channels at angles of $\pm 30^\circ$ to the vertical. The air jets often follow these least-resistance paths. Because the resistance is nonuniform across the layer, the flow tends to adjoin the front or rear window, where the resistance is minimal. In Fig. 4 it is evident that the jets are not continuous, especially their heads. This means that a jet first moves along one wall and then suddenly "switches over" and flows along the other. This conclusion is supported by experiments with larger spheres. Video recording in transmitted light showed that the transparent region is not continuous; the opened pores are usually closed and then are opened again, etc.

Thus, the flow pattern in the layer of spheres turned out to be rather complex because of transverse inhomogeneity. As a result of attraction to the walls, about half of the air volume may not be visible.

Figure 5 shows the initial position (at the left) and a developed flow (at the right) in a nearly horizontal cell. The flow plane was at an angle of about 10° to the horizon. The snapshot was taken from above. The remaining parameters of the experiment are the same as in Fig. 4. The initial distortions of the boundary are caused by capillary effects. Here the shape of the displacement region, agrees, at least qualitatively, with the one expected for an isotropic medium. Typical branching jets can be seen. The same cell viewed from below gives a different pattern with a small number of narrow jets. The difference is explained by the fact that for horizontal or slightly oblique positions of the cell, air forces its way primarily through the upper part of the layer because of buoyancy.

Thus, the analogy with viscous displacement is partly confirmed. Instability of the front and development of jets are observed. At the same time, the flow in plane model cells turned out to be more diversified than might be expected. The flow bears the "imprint" of the symmetry of the anisotropic structure of the model. Only in an almost horizontal layer of spheres, where the "jumps" of jets between the walls is blocked by buoyancy, can one obtain patterns that resemble fractal displacement clusters (although in the viscous flow regime more ramified structures with thin branches are observed [3, 4]). It is not impossible that in a vertical layer of spheres, the flow is similar to the flow in a nearly horizontal layer, and the observed differences are superficial and due only to the fact that the jets are partly hidden in the invisible side of the cell. In horizontal flow, this tendency is inhibited by buoyancy.

2. Anisotropic Flow Model. We restrict ourselves to the simplest case of a square lattice, and first consider its longitudinal orientation with the channels directed along the x and y axes. Here and below, it is more convenient to set the upward direction of displacement along the y axis because gravity is ignored in the model.

For the flow in the lattice of channels, we use the approximation of a continuous medium, in which the characteristic flow dimension should be much larger than the lattice period d. This condition is satisfied at least at the early stages of displacement, where the interface is rather smooth. In flow, the pressure gradient is almost counterbalanced by friction. Otherwise, the inertial terms would be of the order of the pressure gradient, and the flow velocities would be an order of magnitude higher. Therefore, we use a filtration type model, ignoring the inertia of the liquid.

For a typical flow velocity of about 1 m/sec, the Reynolds number calculated from the channel width exceeds 2000, which is sufficient for establishment of a turbulent regime. For a laminar longitudinal flow, estimation using the Poiseuille formula gives velocities higher than 20 m/sec. Therefore, only quadratic friction was taken into account in our analysis.

In lattice models of a porous medium, a special resistance mechanism arises due to the interaction of flows in mutually perpendicular channels. We consider the neighborhood of the intersection of two channels. Let in one of them, for example, the vertical channel, the flow velocity be V. Through the cross section of the entrance transverse channel, the liquid flows with horizontal velocity U, and the same amount of liquid flows out from the exit transverse channel. We emphasize that the average vertical velocities of these flows are different. The vertical velocity of the liquid coming into the region of intersection from the horizontal channel is practically zero, and the vertical velocity of the issuing liquid is about V. To maintain such withdrawal of the vertical momentum from the region of intersection, the vertical pressure gradient should be proportional to the product UV. Having entered the horizontal channel, the liquid loses vertical momentum (transfers it to the wall).

Thus, for fast channel flows, a reasonable approximation is the following system of equations:

$$\frac{\partial p}{\partial y} = -bv|u| - av|v|, \qquad \frac{\partial p}{\partial x} = -bu|v| - au|u|. \tag{5}$$

Here u and v are the average flow velocity components along the x and y axes, respectively, and $a = \alpha\rho/\delta$ and $b = \beta\rho/d$, where d is the lattice period, δ is the channel diameter, and α and β are nondimensional coefficients. In Eqs. (5) the first terms on the right side describes the effect of flow deceleration in a given direction (for example, y) due to the injection of mass from the transverse system of channels (in this case with velocity $|u|$), and β is about 1. The second term describes ordinary square-law friction (the weak dependence of the drag coefficient α on the flow velocity is ignored).

According to (5), the pressure gradient is not antiparallel to the velocity. Generally, when the components are of the same order of magnitude, the first (cross) terms make a marked contribution to the resistance. For $b > a$, they deflect the pressure gradient to the bisector of the quadrant opposite to the one which contains the velocity vector, and for $b < a$, the gradient "is deflected" to the coordinate axis nearest to the velocity direction. It should be noted that anisotropy is conserved for $a = b$ as well. Although, in this case, the gradient is opposite to the velocity direction, the magnitude of the gradient depends on the flow direction (the resistance is maximal in the case of flow along the diagonal). This geometrical property distinguishes the model (5) from well-known anisotropic models of porous media [11, 12]. The difference is due to the fact that in a system of channels, the resistance coefficients are linear in the moduli of the velocity components.

We assume that for the diagonal orientation, the y axis still coincides with the initial direction of displacement, and the x axis coincides with the initial position of the interface. In a coordinate system rotated through an angle of 45°, system (5) leads to rather unwieldy equations. However, for the initial stage of displacement, the system is markedly simplified. If the flow is mainly vertical ($v > 0$ and $|u| < v$), the moduli can be omitted:

$$\frac{\partial p}{\partial y} = -\frac{b(v^2 - u^2) + a(v^2 + u^2)}{\sqrt{2}}, \qquad \frac{\partial p}{\partial x} = -\sqrt{2}\, auv. \tag{6}$$

In experiments, the velocity of displacement V was measured for both orientations of the lattice at an early stage where the motion can be considered one-dimensional (i.e., the horizontal velocity component u is ignored). According to (5), $v = \sqrt{\Delta p/(az)}$, where Δp is the pressure drop and z is the initial height of the liquid column. In the case of longitudinal motion, the average vertical velocity v does not coincide with the velocity of the displacement boundary V, because in the horizontal segments of the channels near the boundary, liquid is practically immovable. Since the vertical jets occupy 60% of the total volume of pores, the relation $v = 0.6V$ is valid with good accuracy. In the diagonal case, from (6) we obtain $v = \sqrt{\sqrt{2}\Delta p/((a+b)z)}$, and the velocity of the boundary can be considered equal to the average vertical velocity: $v = V$. For a pressure drop of 70 kPa, velocities $V_l = (1.65 \pm 0.13)$ m/sec are obtained for longitudinal motion and $V_d = (0.89 \pm 0.075)$ m/sec for diagonal motion. From this, one easily finds the resistance coefficients: $\alpha \approx 0.36$ and $\beta \approx 0.8$.

For longitudinal displacement, the relation between the pressure gradient and the velocity of the jets V is given by $\Delta P/z = \alpha\rho(0.6V)^2/\delta$. The effective resistance coefficient for the channels is $0.36\alpha = 0.13$. This value is several times larger than the value obtained from the well-known relations for smooth pipes ($\alpha \approx 0.02$ for square cross section [15]). Apparently, a considerable contribution comes from the "permeability" of the walls — transverse channels, at whose edges exchange of mass and momentum can occur even in the absence of macroscopic transverse flow.

The relative contribution of resistances due to the transverse injection of mass and friction is given by the relation $b/a \approx 0.75$, which can be treated as a measure of anisotropy of the lattice.

3. Initial Stage of Instability. The increments of perturbation growth at the displacement front can be found from Eqs. (5) and (6), linearized on the perturbation amplitude. For the "diagonal" problem, this procedure is easier. Let a vertical pressure gradient $|\nabla p|_0$ be given in an unperturbed flow. From (6), setting $u \ll v$, we have

$$v = \left(-\frac{\sqrt{2}}{b+a}\,\frac{\partial p}{\partial y}\right)^{1/2}, \qquad u = -\frac{1}{\sqrt{2}av}\,\frac{\partial p}{\partial x}.$$

Assuming that $p = p_0 - y|\nabla p|_0 + p'$ (p_0 is the applied pressure and p' is a small additional variable), in a first order in p' from the continuity equation, we have

$$\frac{\partial^2 p'}{\partial y^2} + \Big(1 + \frac{b}{a}\Big)\frac{\partial^2 p'}{\partial x^2} = 0. \tag{7}$$

Let, at $t = 0$, the shape of the boundary be specified by the equation $y = h\cos(kx)$, and the perturbation amplitude be small: $kh \ll 1$. On the boundary, the total pressure is fixed, so that $p' = |\nabla p|_0 y = |\nabla p|_0 h\cos(kx)$. Extending this condition to the x axis, we obtain a solution of (7) in the form $p' = |\nabla p|_0 h\cos(kx)\exp\left(-\sqrt{1+b/a}\,ky\right)$.

As in the isotropic case with quadratic friction ($\exp(-\sqrt{2}\,ky)$ [13]), the perturbation in the vertical direction damps faster compared to viscous flow ($\exp(-ky)$ [1]).

In an anisotropic medium, the liquid flow velocity is not generally normal to the interface (unlike in an isotropic medium). However, for small-amplitude waves, we can ignore this departure and equate the velocity of the boundary to the vertical component v. We obtain

$$v = \left[\frac{\sqrt{2}|\nabla p|_0}{b+a}\left(1 + kh\sqrt{1+\frac{b}{a}}\,\cos(kx)\right)\right]^{1/2} \approx V\left(1 + \frac{kh}{2}\,\sqrt{1+\frac{b}{a}}\,\cos(kx)\right).$$

Here V is the unperturbed velocity. Hence, for diagonal arrangement of channels, the perturbation amplitude increases under the law $dh/dt = (hkV/2)\sqrt{1+b/a}$. The increment of perturbation growth is $\gamma_d = (Vk/2)\sqrt{1+b/a}$.

In the isotropic case, $\gamma = Vk/\sqrt{2}$ [13]. For an experimental value of $b/a \approx 0.75$, the difference between the increments is about 7% (within the experimental spread).

Similarly for longitudinal flow from (5) for $u \ll v$, we obtain

$$v = \Big[-\frac{1}{a}\Big(\frac{\partial p}{\partial y} + \Big|\frac{\partial p}{\partial x}\Big|\Big)\Big]^{1/2}, \qquad u = -\frac{1}{bv}\,\frac{\partial p}{\partial x}.$$

Again, using the continuity equation, in a first order in the perturbation p', we have

$$\frac{\partial^2 p'}{\partial y^2} + \operatorname{sgn}\Big(\frac{\partial p}{\partial x}\Big)\frac{\partial^2 p'}{\partial x\,\partial y} + \frac{2a}{b}\,\frac{\partial^2 p'}{\partial x^2} = 0. \tag{8}$$

This equation is much more complicated than (7) because of the presence of the discontinuity coefficient $\operatorname{sgn}(\partial p/\partial x)$, which is equal to ± 1, depending on the sign of $\partial p/\partial x$. This coefficient can be replaced by $\operatorname{sgn}(\partial p'/\partial x)$ since in the unperturbed flow, $\partial p/\partial x = 0$.

Regularization of Eq. (8) requires additional assumptions. In addition, one cannot state with confidence that Eq. (8) describes instability of longitudinal flow because the displacement process is complicated by the obvious incompleteness of the displacement. Therefore, in the longitudinal case, the increment was not obtained.

Visually, the growth rates of small perturbations for longitudinal (see Fig. 2a) and diagonal (see Fig. 2c) orientations differ markedly: for diagonal displacement, the growth is more rapid. To estimate this difference, we digitized the experimental data and subjected them to a harmonic analysis:

$$y(x) = A_0 + \sum A_n \cos \frac{2n\pi x}{l} + \sum B_n \sin \frac{2n\pi x}{l}.$$

Here l is the cell width and n = 1–20 is the harmonic number. The amplitude of a given harmonic $C_n = (A_n^2 + B_n^2)^{1/2}$ increases under the law

$$\ln (C_n(t)/C_n(0)) = n\pi H\theta/l, \tag{9}$$

where $H = Vt$ is the average displacement of the boundary and the coefficient θ depends on the orientation of the lattice. For diagonal displacement, the theoretical value $\theta_d = \sqrt{1 + b/a} \approx 1.32$. The harmonic amplitudes and the average displacement H were determined within 1/30 sec from the beginning of the process (the first 5 frames). Among all waves, two highest in amplitude were chosen. The main harmonic ($n = 1$) was most pronounced. The next highest amplitude was usually found for the second harmonic but sometimes for the third or fourth harmonics. The amplitudes of the remaining waves were about δ or less, i.e., insufficient to determine the increments. Assuming, in accordance with (9), that $\ln (C_n(t)/C_n(0)) \sim H(t)$, we calculated the geometrical coefficients θ_d and θ_l by the least square procedure. The average values obtained are equal to $\theta_l = 0.69 \pm 0.11$ and $\theta_d = 1.18 \pm 0.17$.

Despite the crudeness of the model, the theoretical value of θ_d is close to the experimental one, especially bearing in mind the considerable spread of experimental data. Unfortunately, the available data were not sufficient for more detailed processing. First, the spectral interval in which the macroscopic approach is valid is not too wide. The applicability of the continual model is limited by the condition $kd = 2\pi nd/l \leqslant 1$, which is satisfied for $n \leqslant 5$. Second, the phase of linear growth was not long enough to allow more accurate determination of the growth rate.

4. Developed Stage of Instability. In square lattices, unlike in the isotropic case, the displacement pattern is not fractal for both channel orientations. Marked branching of fingers was not observed. Qualitatively, this can be explained as follows.

For longitudinal displacement, the resistance to the finger growth along its axis (y direction) reduces to pure friction: $\partial p/\partial y \approx -av^2$. The side expansion of the finger in the x direction is counteracted not only by friction but also by the transverse effect: $\partial p/\partial x \approx -bVu - au^2$. The velocity V is induced by motion of the finger pedestal, i.e., the main displacement front, and has the same order of magnitude as the growth rate of the top. In addition, the transverse pressure gradient is lower than the longitudinal one, and the flow velocity u in the lateral direction is low. The gradient components are of the same order of magnitude only near the top of the finger that has kept ahead of the neighbors. Because of the rather slow development of longitudinal instability, this state for each of the transverse channels is short. As a result, noticeable lateral growth of the finger does not occur.

For diagonal orientation, the instability growth is fast, and the fingers reach the wedge stage rapidly. After that, their shape becomes more stable because the motion of the boundaries is nearly longitudinal. [It should be noted that this propagation is not exactly longitudinal because the liquid is completely displaced (see Fig. 3).] Experiment shows that the wedges do not develop smaller branches. Rather, small wedges merge into larger formations.

At the final stage, one large wedge forms in the central part of the cell. This can be explained by the fact that the outlets strongly affect the flow at the bottom of the cell, as a result of which the resistance along the cell axis decreases. Faster propagation along the middle of the cell is also observed for longitudinal displacement: at the end of the process, the system of jets in Fig. 2a and b resembles a hand.

Thus, anisotropy blocks the fractal mode, at least, for experiments of the present scale (when the transverse dimension of the cell was about 33 lattice periods). It is unlikely that the fractal regime of displacement can occur in experiments of larger scale because no finger branching is observed.

In the case of a layer of spheres, the arrangement of channels is closer to the diagonal one. However, because of the greater geometrical complexity of the pore space, the flow structure in this model is more diversified compared to regular lattices, in particular, due to bifurcations of jets between the walls. The

amount of the liquid that is not displaced from the porous medium is larger in this case than in a diagonal lattice.

In view of the marked anisotropy of the layer of spheres, the results obtained in a nearly horizontal cell are somewhat surprising (see Fig. 5). In this case, the structure has a "nearly" fractal form. It is believed that near the wall, the anisotropy of the model is not high enough to suppress branching during displacement, which is natural for the isotropic case. In order that the branches be seen, the flow should follow the plane of observation.

5. Conclusions. Fast displacement of a dense liquid by a gas is unstable. In an anisotropic medium, the growth rate of small-amplitude perturbations depends on the flow direction. Development of the instabilities leads to the formation of jets whose shape is determined by the symmetry of the medium. Fractal structures typical of a linear filtration regime were not observed in square lattices of channels. Nevertheless, the displacement is substantially nonuniform and the fingers are markedly ahead of the middle front. In a nearly horizontal layer of spheres, the structures obtained are similar to fractal structures but are denser than those in the case of isotropic displacement.

The proposed model (5) provides an understanding of the nature of the quadratic "inertial" resistance component not only for isotropic media but also for isotropic porous media. Pore flow can be imagined as a set of jets with average velocity V. The random transverse velocity component is generally also of the order of V. Transverse mass exchange between the jets carries part of the liquid from the channels having nearly longitudinal direction to the transverse channels, in which the directional flow is decelerated. Such losses of longitudinal momentum may be one of the basic mechanisms responsible for the quadratic resistance in a porous medium.

REFERENCES

1. P. G. Saffman and G. I. Taylor, "The penetration of a fluid into a porous medium or Hele Shaw cell containing a more viscous liquid," *Proc. Roy. Soc., London*, **A 245**, No. 1242, 311–329 (1958).
2. L. Paterson, "Radial fingering in a Hele Shaw cell," *J. Fluid Mech.*, **113**, 513–529 (1981).
3. K. J. Måløy, J. Feder, and T. Jøssang, "Viscous fingering fractals in porous media," *Phys. Rev. Lett.*, **55**, No. 24, 2688–2691 (1985).
4. R. Lenormand, E. Touboul, and C. Zarcone, "Numerical models and experiments on immiscible displacements in porous media," *J. Fluid Mech.*, **189**, 165–187 (1988).
5. G. Daccord, J. Nittman, and H. E. Stanley, "Radial viscous fingers and diffusion-limited aggregation: Fractal dimension and growth sites," *Phys. Rev. Lett.*, **56**, No. 4, 336–339 (1986).
6. L. Paterson, "Diffusion-limited aggregation and two-fluid displacement in porous media," *Phys. Rev. Lett.*, **52**, No. 18, 1621–1624 (1984).
7. T. A. Witten and L. M. Sander, "Diffusion-limited aggregation, a kinetic critical phenomenon," *Phys. Rev. Lett.*, **47**, No. 19, 1400–1403 (1981).
8. T. A. Witten and L. M. Sander, "Diffusion-limited aggregation," *Phys. Rev., B*, **27**, No. 9, 5686–5697 (1983).
9. L. Niemeyer, L. Pietronero, and H. J. Wiesmann, "Fractal dimension of dielectric breakdown," *Phys. Rev. Lett.*, **52**, No. 12, 1033–1036 (1984).
10. C. Evertsz, "Self-affine nature of dielectric-breakdown model clusters in a cylinder," *Phys. Rev. A*, **41**, No. 4, 1830–1842 (1990).
11. A. É. Sheideger, *Physics of Fluid Flows through Porous Media* [in Russian], Gostoptekhizdat, Moscow (1960).
12. *Progress of Research on Filtration Theory in the USSR* [in Russian], Nauka, Moscow (1969).
13. A. P. Ershov, A. L. Kupershtokh, and A. Ya. Dammer, "Fingering in the fast flow through a porous medium," *J. Physique II France*, **3**, No. 7, 955–959 (1993).
14. V. A. Arkhipov, V. N. Vilyunov, E. A. Kozlov, and V. F. Trofimov, "Convective combustion in ordered porous structures," *Fiz. Goreniya Vzryva*, **22**, No. 4, 25–30 (1986).
15. G. Schlichting, *Boundary Layer Theory*, McGraw-Hill, New York (1968).